Materials Chemistry and Physics 123 (2010) 241–246

Contents lists available at ScienceDirect

Materials Chemistry and Physics

journal homepage: www.elsevier.com/locate/matchemphys

Effect of carbon content on microstructure and corrosion behavior of hypereutectic Fe–Cr–C claddings

Chia-Ming Chang[a], Chih-Chun Hsieh[a], Chi-Ming Lin[a], Jie-Hao Chen[a], Chih-Ming Fan[b], Weite Wu[a,*]

[a] Department of Materials Science and Engineering, National Chung Hsing University, 250 Kuo-Kuang Road, Taichung, Taiwan
[b] Kuang Tai Metal Industrial Co., Ltd., 8 Lu-Ke Third Road, Lujhu Township, Kaohsiung, Taiwan

ARTICLE INFO

Article history:
Received 1 June 2009
Received in revised form 5 March 2010
Accepted 6 April 2010

Keywords:
Carbides
Welding
Microstructure
Corrosion

ABSTRACT

The aim of this study was to examine the influence of carbon content on the microstructures and corrosion characteristics. The results showed that the hypereutectic microstructure comprised primary $(Cr,Fe)_7C_3$ carbides and the eutectic colonies [γ-Fe + $(Cr,Fe)_7C_3$]. The amounts of primary $(Cr,Fe)_7C_3$ carbides increased from 33.81 to 86.14% when carbon content increased from 3.73 to 4.85 wt%. The corrosion resistance of the hypereutectic alloy with 4.85 wt% C was about 20 times higher than that with 3.73 wt% C. The galvanic corrosion occurred in all claddings due to difference of corrosion potential between primary carbide and austenite. The dense distribution of primary carbides could retard the austenitic matrix from selective corrosion. The austenite dissolved the Fe^{2+} ions and formed a Cr_2O_3 film under 3.5% NaCl aqueous solution.

1. Introduction

The superior abrasive and erosive wear resistance of Fe–Cr–C alloys results from great amounts of hard carbides with excellent corrosion resistance. The abrasion wear resistance is reported to be dependent upon not only type, morphology, amount, and distribution pattern of the carbides precipitated from the melt, but also the type of matrix structure [1]. In general, the microstructure observations of Fe–Cr–C alloys have shown that these types of materials contain hypoeutectic, eutectic and hypereutectic structures [2–4]. The hypoeutectic microstructures consist of primary dendrites of austenite (γ) phase and eutectic colonies (γ + M_7C_3). The hypereutectic microstructures include the primary M_7C_3 carbides and eutectic colonies (γ+ M_7C_3).

Much attention has been focused on the wear behavior of Fe–Cr–C alloys and several models have also been developed for the microstructure–property relationship of these alloys [5–11]. However, the slurries are often corrosive in the oil sand production. Erosion corrosion causes a serious problem for the oil sands industry where handling and processing of essentially silica-based solids results in extremely severe corrosion and wear conditions [12]. The Cr_7C_3 is well known for its excellent combination of high hardness, excellent wear resistance as well as good corrosion and oxidation resistance, so it has been widely used as the reinforcing phase in the composite coatings [13–16]. However, the information on the performance of these alloys in the corrosive environments is yet limited in the open literature [17,18]. Therefore, it is very significant to utilize this carbide to improve the corrosion and wear properties.

The purpose of this study was to investigate the effect of carbon contents on the microstructures and corrosion resistance of hypereutectic Fe–Cr–C claddings. The results of this research may provide the criteria to be used for selecting the cladding surface for corrosion applications depending on the microstructural features of its microstructures.

2. Experimental procedures

The substrates (150 mm × 100 mm × 10 mm) for cladding the hypereutectic Fe–Cr–C claddings were prepared from ASTM A36 steel plates, which were ground and cleaned with acetone before welding. Various amounts of graphite and chromium powders were added into flux cored wires to obtain hypereutectic Fe–Cr–C claddings with various carbon contents. These claddings were usually deposited in three layers to avoid dilution of top layer by substrate. Equipment was used in the present study, as illustrated in Fig. 1. These claddings were deposited using a flux cored arc welding technique with 2.8 mm diameter flux cored wire; the welding conditions were 350 A, 33 V with travel speed of 0.005 m s^{-1}, the interpass temperature being 250 °C.

The chemical compositions of claddings were analyzed quantitatively by use of the optical emission spectroscopy (OES), as listed in Table 1. OES was a method of chemical analysis that used the intensity of light emitted from a spark at a particular wavelength to determine the quantity of an element in a sample. The wavelength of the atomic spectral line gave the identity of the element while the intensity of the emitted light was proportional to the number of atoms of the element. Microstructural evolutions were carried out on the top surface of the claddings after polishing and etching. The etching solution was aqua regia (the ratio of HCl and HNO_3 was 3:1). The microstructure of these claddings was characterized using the optical microscope (OM). This study used image analysis software to analyze

* Corresponding author. Tel.: +886 4 22879000; fax: +886 4 22857017.
E-mail address: wwu@nchu.edu.tw (W. Wu).

0254-0584/$ – see front matter © 2010 Elsevier B.V. All rights reserved.
doi:10.1016/j.matchemphys.2010.04.003

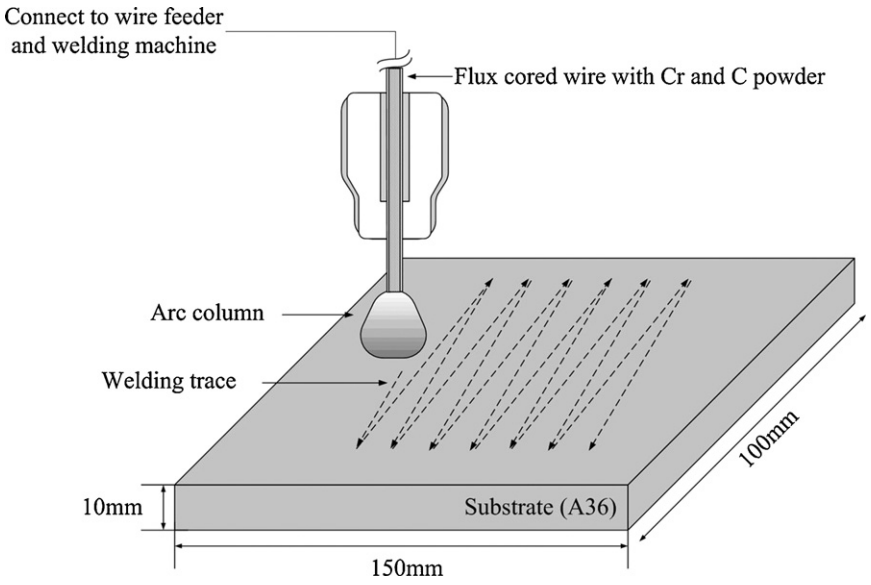

Fig. 1. Scheme diagram of flux cored wire arc welding for depositing the Fe–Cr–C claddings.

quantitatively the amounts of primary $(Cr,Fe)_7C_3$, and measured result was shown in Table 1. Ten pictures at 50 magnifications were taken for quantitative amounts of primary $(Cr,Fe)_7C_3$. The chemical composition of each phase was carried out by energy dispersive spectroscopy (EDS).

Each specimen was covered in waterproof tape, leaving an exposed area of 1 cm^2 on the cladding surface under 3.5 wt% NaCl solution at 30 °C was used as a corrosion medium. Potentiodynamic polarization tests were performed to evaluate the overall corrosion behavior of the specimens. A typical three-electrode cell was used for electrochemical corrosion tests. Electrical current from a potentiostat shifted a working electrode from its free corrosion potential or E_{corr} to a potential value determined by the magnitude of the current. Changing an electrode potential from its E_{corr} was referred to as polarization. To maintain electrode electrical neutrality, electrical current had to be concurrently drawn from a test electrode when current was supplied by potentiostat to a counter-electrode. The working electrode polar-

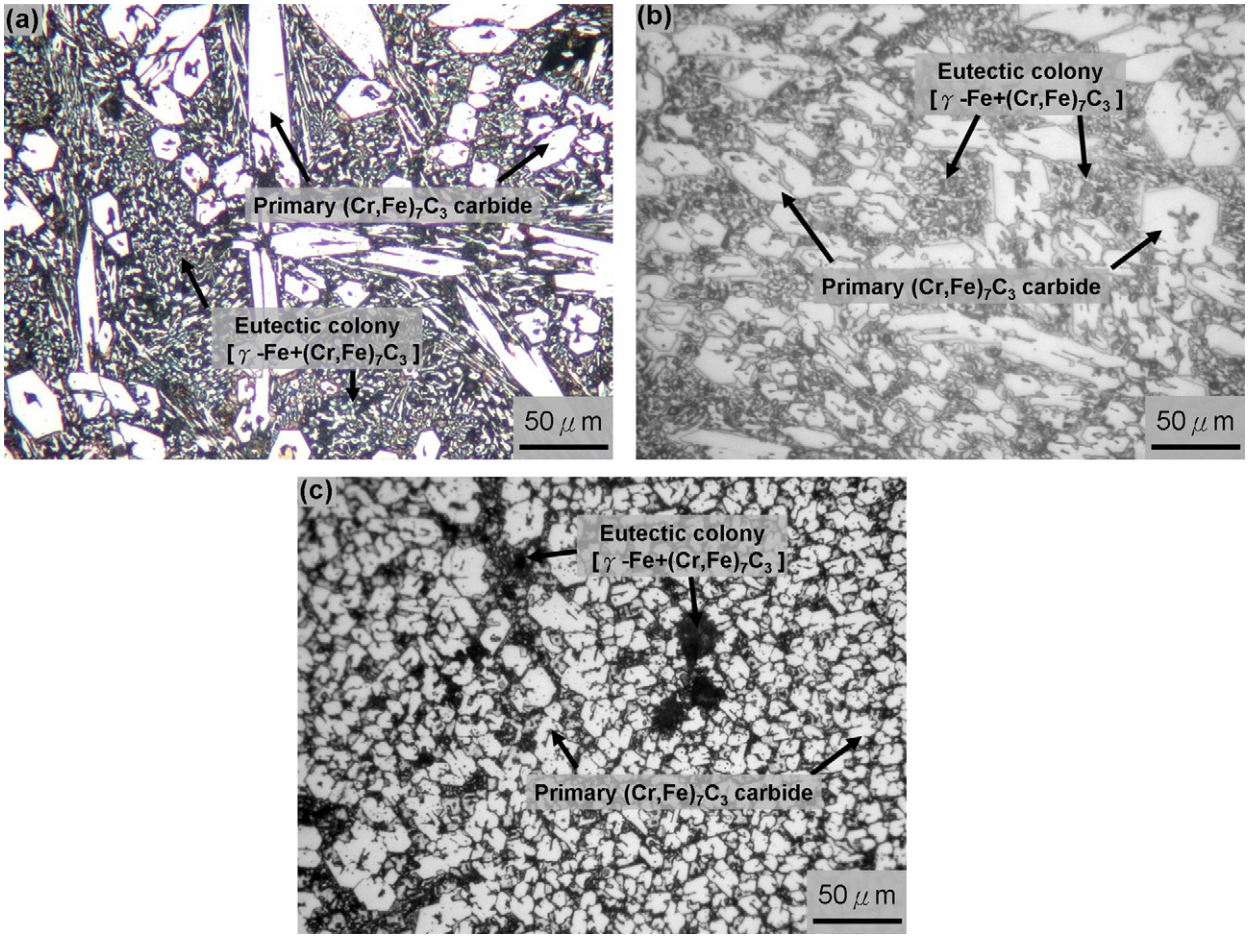

Fig. 2. Microstructure of hypereutectic Fe–Cr–C claddings with various C contents: (a) 3.73 wt% C, (b) 4.21 wt% C and (c) 4.85 wt% C.

Table 1
Chemical compositions and amounts of primary $(Cr,Fe)_7C_3$ carbides for claddings and substrate.

Claddings	Composition (wt%)					Amount of primary $(Cr,Fe)_7C_3$ carbides (%)
	C	Si	Mn	Cr	Fe	
Substrate (A36)	0.18	0.15	0.55	0.09	bal.	–
Cladding A	3.73	2.28	2.33	26.70	bal.	33.81
Cladding B	4.21	2.00	2.26	27.08	bal.	61.19
Cladding C	4.85	1.96	2.28	27.31	bal.	86.14

ization was measured as a potential difference between the reference and working electrode. The polarization resistance was measured with a potential scanning rate of 0.5 mV s^{-1} within the potential range of $E_{oc} \pm 10$ mV. The E_{oc} is the open circuit potential of material under the test condition. The silver–silver chloride electrode was regarded as a reference electrode. After polarization test, the corroded surface was observed by OM.

3. Results and discussion

3.1. Microstructure

Previous researchers [19–22] indicated that the morphology of M_7C_3 carbides included blade-like and rod-like shape in Fe–Cr–C claddings. Fig. 2a–c presents the microstructures of hypereutectic Fe–Cr–C claddings with various carbon contents. The primary $(Cr,Fe)_7C_3$ carbides and the eutectic colonies [γ-Fe + $(Cr,Fe)_7C_3$] occurred in all hypereutectic Fe–Cr–C claddings. According to the liquidus projection for the Fe–Cr–C ternary system [23–26], the chemical composition of all claddings located in M_7C_3 liquidus surface, as shown in Fig. 3. Therefore, the molten liquid phase transformed into the $(Cr,Fe)_7C_3$ carbides as primary phase during solidification. Then, the eutectic reaction [L → γ-Fe + $(Cr,Fe)_7C_3$] proceeded as the temperature of molten liquid decreased at the eutectic point. Finally, primary $(Cr,Fe)_7C_3$ carbides and the eutectic colonies [γ-Fe + $(Cr,Fe)_7C_3$] were remained under the room temperature.

Based on Fig. 2, the amounts of primary $(Cr,Fe)_7C_3$ carbides for each cladding were measured by image analysis, as shown in Table 1. The amounts of primary $(Cr,Fe)_7C_3$ carbides in claddings increased from 33.81 to 86.14% when carbon content increased from 3.73 to 4.85 wt%. This could be explained by the viewpoint of the degree of undercooling. For an off-eutectic composition, the liquidus temperature was much higher than the eutectic temperature. Thus, the corresponding primary phase was high undercooling and tends to grow faster than the eutectic [3]. Moreover, the addition of carbon lowered the eutectic temperature in Fe–Cr–C alloy

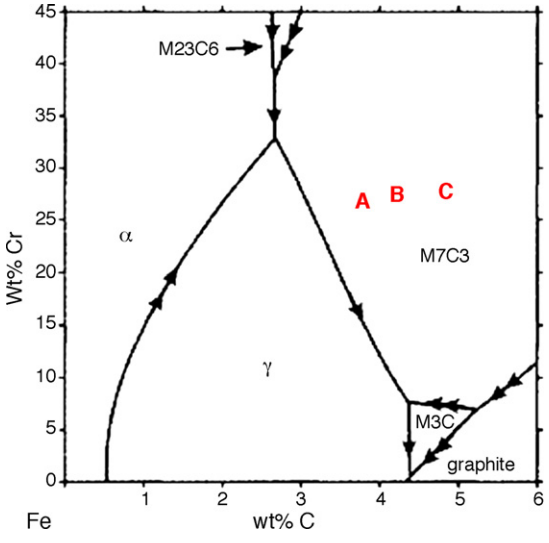

Fig. 3. Liquidus projection for the Fe–Cr–C ternary system [23–26].

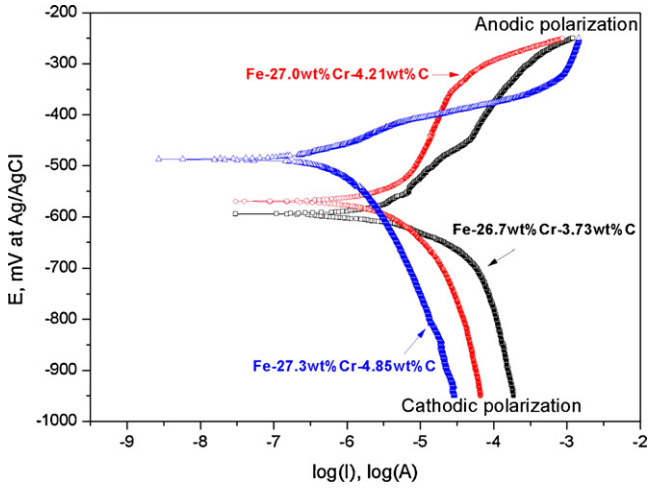

Fig. 4. Potentiodynamic polarization curves of claddings with various C contents under 3.5 wt% NaCl at 30 °C condition.

[27,28]. The lower eutectic temperature promoted the growth of primary carbides due to the high degree of undercooling. Therefore, the amount of primary $(Cr,Fe)_7C_3$ carbides increased and that of eutectic colonies decreased under the higher carbon contents.

3.2. Potentiodynamic polarization curves

Generally, the corrosion reaction of iron-base alloys in a solution containing dissolved oxygen with near-neutral pH could be written as follows [29]:

$$\text{Anodicreaction}: Fe \rightarrow Fe^{2+} + 2e^- \quad (1)$$

$$\text{Cathodicreaction}: (1/2)O_2 + 2H_2O + 2e^- \rightarrow 2OH^- \quad (2)$$

$$\text{Overallreaction}: Fe + 2H_2O + O_2 \rightarrow 2Fe^{2+} + 4OH^- \rightarrow 2Fe(OH)_2\downarrow \quad (3)$$

Dynamic polarization diagrams in 3.5% NaCl aqueous solution for the hypereutectic Fe–Cr–C cladding with various carbon contents were shown in Fig. 4. It was evident that the corrosion potential of the cladding with 4.85% C (−486 mV) was higher than that for 3.73% C (−594 mV). This indicated that more carbon content led to nobler corrosion potential for hypereutectic Fe–Cr–C claddings. The corrosion potential of $(Cr,Fe)_7C_3$ carbide in hypereutectic Fe–Cr–C cladding was believed to be nobler than that of austenite. According to EDS analysis (Table 2), the chromium

Table 2
EDS results of primary $(Cr,Fe)_7C_3$ carbides and austenite phase.

Phase	Composition (wt%)				
	C	Si	Mn	Cr	Fe
$(Cr,Fe)_7C_3$	10.23	0.00	2.11	51.59	36.07
Austenite	0.82	4.33	2.08	8.68	84.09

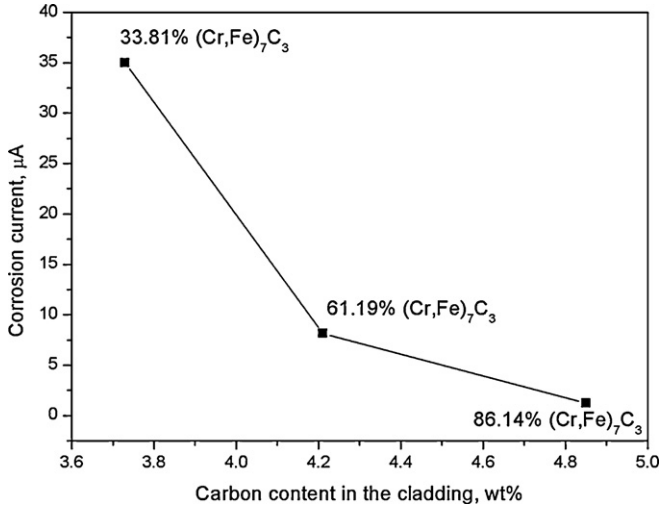

Fig. 5. Relationship between corrosion current and carbon content for hypereutectic Fe–Cr–C claddings.

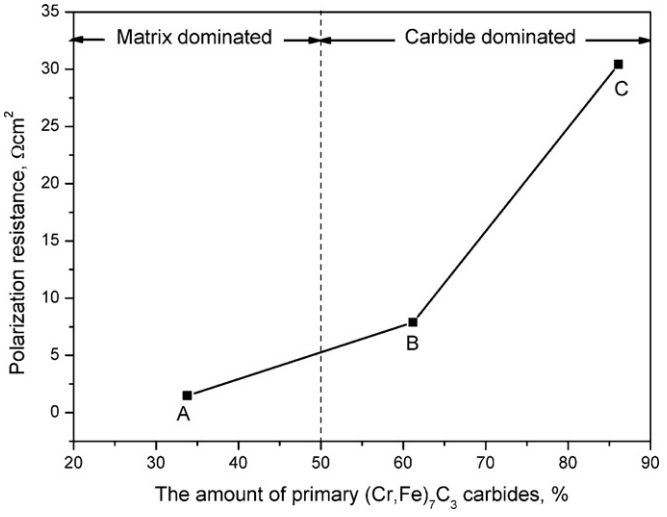

Fig. 6. Relationship between the corrosion resistance and the amount of primary $(Cr,Fe)_7C_3$ carbide.

content of $(Cr,Fe)_7C_3$ (51.5 wt%) is higher than that of austenite (8.6 wt%). Therefore, the $(Cr,Fe)_7C_3$ is nobler than austenite. As a result, the more $(Cr,Fe)_7C_3$ carbides could move from the corrosion potential of cladding to nobler direction.

Tafel extrapolation method was used to determine corrosion current of these claddings. Tafel extrapolation method was introduced to illustrate the application of mixed potential theory to aqueous corrosion. Fig. 4 shows polarization data for each cladding with extrapolation of the cathodic Tafel slope back to the corrosion potential, E_{corr}. The intersection gave the corrosion rate or corrosion current density, I_{corr}, as was demonstrated from mixed potential theory. The relationship between corrosion current and the carbon

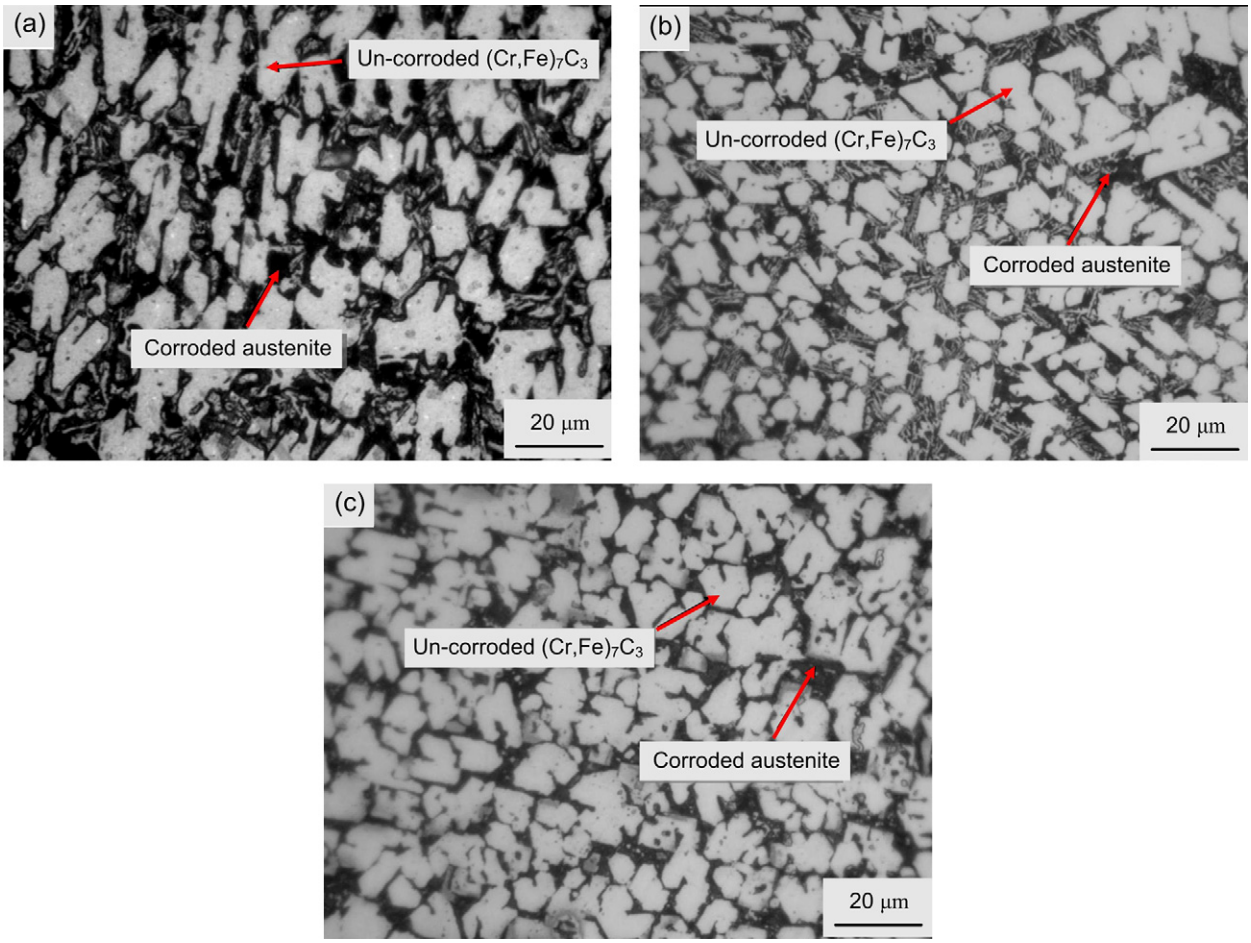

Fig. 7. Corroded surfaces of claddings with various C contents after polarization test: (a) 3.73 wt% C, (b) 4.21 wt% C and (c) 4.85 wt% C.

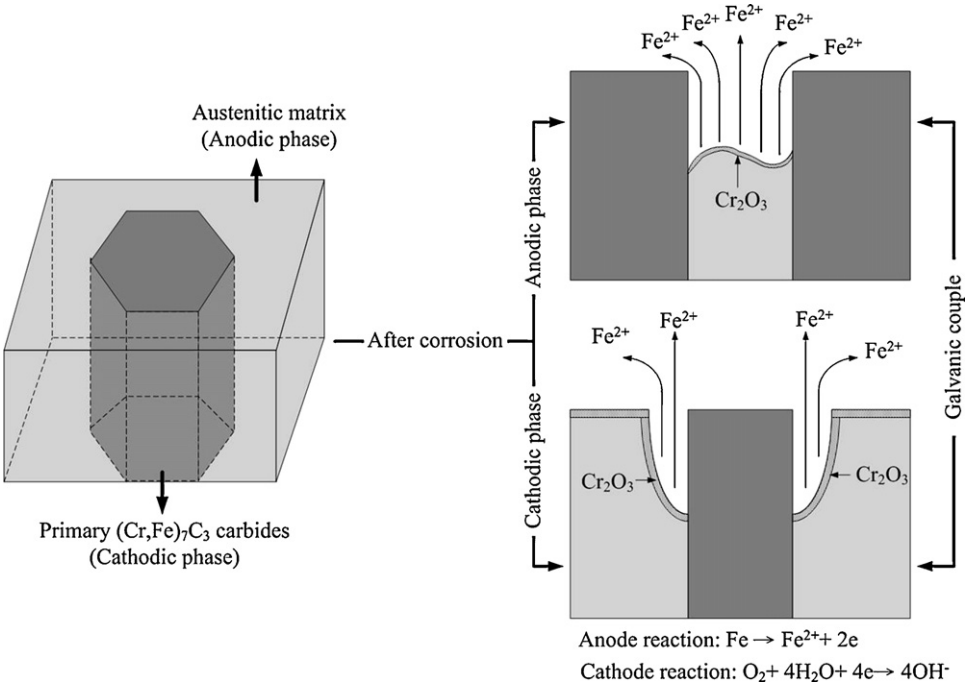

Fig. 8. Illustration of galvanic corrosion for hypereutectic Fe–Cr–C cladding.

content of claddings were shown in Fig. 5. The corrosion current of the cladding with 4.85 wt% C (1.24 μA) was reduced to about 1/30 of the cladding with 3.73 wt% C (35 μA). Obviously, the higher carbon content was effective in increasing corrosion resistance in Cl^- containing environment.

The polarization resistance (R_p) was used in the current investigation to evaluate the corrosion resistance of hypereutectic Fe–Cr–C claddings since the corrosion current (I_{corr}) could relate to the polarization resistance, their relationship can be written as follows:

$$R_p = \frac{B}{I_{corr}}, \quad (4)$$

where B was a constant depending on the corrosion system [30]. Fig. 6 indicates the relationship between corrosion resistance and the amount of primary $(Cr,Fe)_7C_3$ carbides. It could be seen that the values of polarization resistance increased from 1.49 to 30.43 $\Omega\,cm^2$ when the amount of primary $(Cr,Fe)_7C_3$ carbides increased from 33.81% to 86.14%. The corrosion resistance of the cladding with 86.14% carbides was about 20 times higher than that with 33.81% carbides.

Consequently, the higher polarization resistance, nobler corrosion potential and lower corrosion current indicated a better corrosion resistance for cladding. As a result, the best corrosion resistance was obtained in the cladding with 4.85 wt% C, but the worst one occurred in the cladding with 3.73 wt% C. The corrosion resistance of the hypereutectic cladding with 4.85 wt% C was approximately 20 times higher than that with 3.73 wt% C. The chromium carbide was passive, but the surrounding chromium-depleted austenite was attacked. The area of attacked austenitic matrix relatively decreased as the amount of primary $(Cr,Fe)_7C_3$ carbides increased. Therefore, the corrosion resistance of cladding was enhanced by the great amounts of primary $(Cr,Fe)_7C_3$ carbides.

On the other hand, it was noted that corrosion resistance suddenly increased from 1.49 to 7.88 Ωcm^2 when the amount of primary $(Cr,Fe)_7C_3$ carbides increased from 33.81% to 66.14%. The corrosion resistance was dominated by the austenite while the amount of primary $(Cr,Fe)_7C_3$ carbides was below 50%. As the amount of primary $(Cr,Fe)_7C_3$ exceeded 50%, the influence of resistant $(Cr,Fe)_7C_3$ carbides on the corrosion resistance was predominant. Consequently, the corrosion resistance increased rapidly with increasing of the amount of primary $(Cr,Fe)_7C_3$ carbides as the amount of primary $(Cr,Fe)_7C_3$ carbides exceeded 50%.

3.3. Corrosion behavior

After polarization tests in 3.5% NaCl aqueous solution, the galvanic corrosion was observed, as shown in Fig. 7a–c. These results indicated that the primary $(Cr,Fe)_7C_3$ carbides exhibited more corrosion resistance than the austenite. Otherwise, the austenitic matrix were attacked and corroded. Fig. 8 illustrates the schematic diagram of the galvanic corrosion for hypereutectic Fe–Cr–C claddings. Because the primary $(Cr,Fe)_7C_3$ carbides was more corrosion resistant, the corrosion potential of primary $(Cr,Fe)_7C_3$ carbides was higher than that of austenitic matrix. The primary $(Cr,Fe)_7C_3$ carbides became nobler and the austenitic matrix became more active. Therefore, The primary $(Cr,Fe)_7C_3$ carbides and austenitic matrix caused a galvanic couple. However, the amount or area of each phase was also important for the corrosion behavior. The area of corroded austenitic matrix was less and the corrosion resistance will be improved at the same time. As long as the resistant primary $(Cr,Fe)_7C_3$ carbides increased, the corrosion resistance of claddings enhanced. Finally, the corrosion resistance was proportioned to the amount of resistant phase. Besides, the Fe atoms of γ-Fe were dissolved into 3.5% NaCl solution during the electrochemical condition. The Fe^{2+} reacted with OH^- to produce the $Fe(OH)_2$. Simultaneously, the Cr atoms of γ-Fe were combined with O_2 to form the Cr_2O_3. Fig. 9a and b shows the Pourbaix diagrams of iron and chromium [30], which indicated the iron atoms dissolved Fe^{2+} ions and chromium atoms formed the Cr_2O_3 in pH = 7 with the potential between −1.0 and −0.2 mV. Therefore, it was concluded that the γ-Fe dissolved into the Fe^{2+} ions and Cr_2O_3 film.

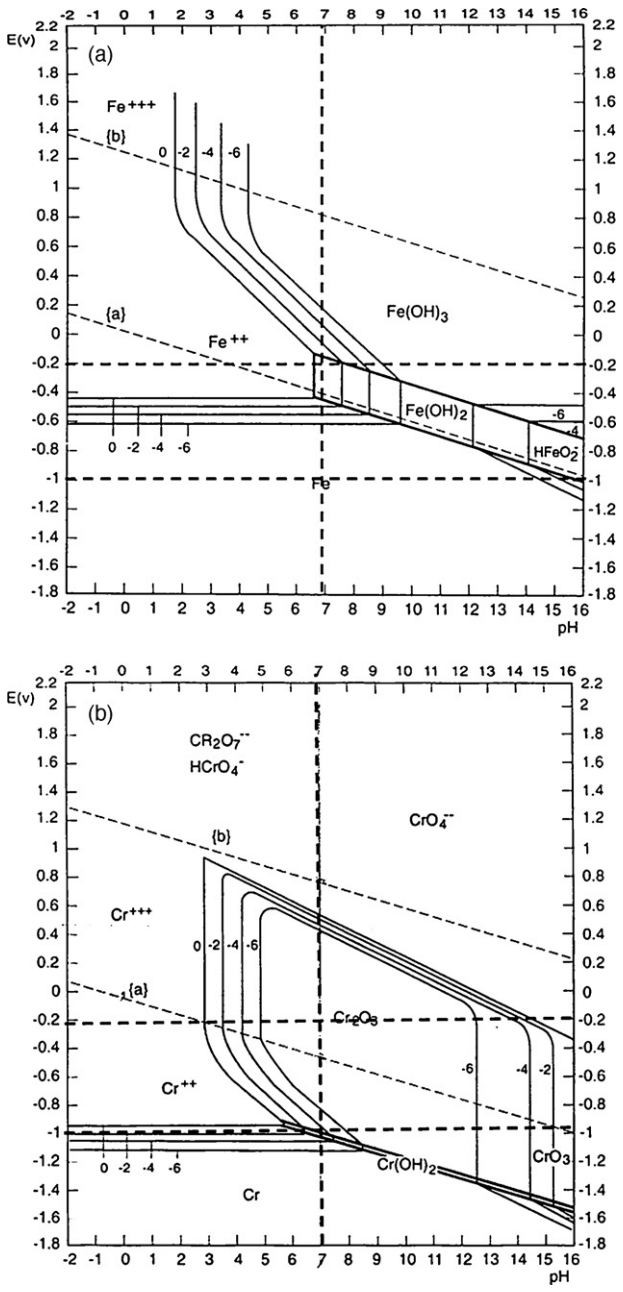

Fig. 9. Pourbaix diagram of (a) iron and (b) chromium [30].

4. Conclusions

In this study, FCAW process was utilized to clad hypereutectic Fe–Cr–C claddings on the ASTM A36 steel. The claddings were designed to various carbon contents to discuss the microstructure and corrosion behavior. Moreover, the relationship between microstructure and corrosion behavior of claddings was discussed. The results can be summarized as follows:

1. The series of hypereutectic Fe–Cr–C claddings consisted of the primary $(Cr,Fe)_7C_3$ carbides and the eutectic colonies [γ-Fe + $(Cr,Fe)_7C_3$]. The amount of primary $(Cr,Fe)_7C_3$ carbides increased with the carbon content of hypereutectic Fe–Cr–C cladding.
2. The increase in carbon contents promoted the corrosion potential drifted towards noble side and reduced the corrosion current. As a result, the increment of carbon content can improve the corrosion resistance of the hypereutectic Fe–Cr–C claddings.
3. The corrosion form of hypereutectic Fe–Cr–C cladding was galvanic corrosion. The austenitic matrix became more active, and the primary $(Cr,Fe)_7C_3$ carbides became nobler.
4. The corrosion resistance was proportioned to the amount of resistant primary $(Cr,Fe)_7C_3$ carbides.

Acknowledgement

The authors are obligated to thank the National Science Council and Ministry of Economic Affairs of Taiwan, ROC for their financial support under projects numbered 98-EC-17-A-08-S1-117, NSC98-2622-E-005-006-C2, and NSC98-2221-E-005-027.

References

[1] Y. Matsubara, N. Sasaguri, K. Shimizu, S.K. Yu, Wear 250 (2001) 502.
[2] L. Lu, H. Soda, A. McLean, Mater. Sci. Eng. A 347 (2003) 214.
[3] C. Fan, M.C. Chen, C.M. Chang, W. Wu, Surf. Coat. Technol. 201 (2006) 908.
[4] C.W. Kuo, C. Fan, S.H. Wu, W. Wu, Mater. Trans. 48 (2007) 2324.
[5] C.M. Chang, C.M. Lin, C.C. Hsieh, J.H. Chen, W. Wu, J. Alloys Compd. 487 (2009) 83.
[6] S. Buytoz, M.M. Yildirim, H. Eren, Mater. Lett. 59 (2006) 607.
[7] Y.F. Liu, Z.Y. Xia, J.M. Han, G.L. Zhang, S.Z. Yang, Surf. Coat. Technol. 201 (2006) 863.
[8] C.M. Lin, C.M. Chang, J.H. Chen, C.C. Hsieh, W. Wu, Metall. Mater. Trans. A 40A (2009) 1031.
[9] C.M. Chang, C.M. Lin, C.C. Hsieh, J.H. Chen, C.M. Fan, W. Wu, Mater. Chem. Phys. 117 (2009) 257.
[10] A. Neville, F. Reza, S. Chiovelli, T. Revega, Metall. Mater. Trans. A 37A (2006) 2339.
[11] C.M. Chang, Y.C. Chen, W. Wu, Tribol. Int. 43 (2010) 929.
[12] H.M. Clark, R.J. Llewellyn, Wear 250 (2001) 32.
[13] A.F. Zhang, J.D. Xing, L. Fang, J.Y. Su, Wear 257 (2004) 198.
[14] P.Q. La, Q.J. Xue, W.M. Liu, Wear 249 (2001) 93.
[15] C.T. Liu, J.O. Steigler, F.H. Sam Fores, Metal Handbook, 10th ed., The Materials Information Society, USA, 1990, p. 913.
[16] S. Frangini, A. Masci, A.D. Bartolomeo, Surf. Coat. Technol. 149 (2002) 279.
[17] R.B. Davis, Microstructural Relationship to Flow Accelerated Corrosion, Code and Standard for Quality Engineering, ASME, Minneapolis, MN, 1994, p. 3.
[18] Z. Yue, P. Zhou, J. Shi, Wear of Materials, ASME, New York, 1987, p. 763.
[19] S. Chatterjee, T.K. Pal, Wear 255 (2003) 417.
[20] G.L.F. Powell, R.A. Carlson, V. Randle, J. Mater. Sci. 29 (1994) 4889.
[21] S. Atamert, H.K.D.H. Bhadeshia, Mater. Sci. Eng. A 130 (1990) 101.
[22] A. Lesko, E. Navera, Mater. Charact. 36 (1996) 349.
[23] G.V. Raynor, V.G. Rivlin, Phase Equilibria in Iron Ternary Alloys, The Institute of Metals, The Bath Press, UK, 1988, p. 143.
[24] K. Bungardt, E. Kunze, E. Horn, Arch. Eissenhüttenwes 29 (1958) 193.
[25] N.R. Griffing, W.D. Forgeng, G.W. Healy, Trans. TMS-AIME 224 (1962) 148.
[26] R.S. Jackson, J. Iron Steel Inst. 208 (1970) 163.
[27] O.N. Dogan, J.A. Hawk, G. Laird II, Metall. Mater. Trans. A 28 (1997) 1315.
[28] X. Liu, H. Wang, D. Li, Y. Wu, Surf. Coat. Technol. 201 (2006) 2414.
[29] B. Lu, J. Luo, S. Chiovelli, Metall. Mater. Trans. A 37 (2006) 3029.
[30] D.A. Jones, Principles and Prevention of Corrosion, Upper Saddle River, NJ, 1996, p. 80.